Supplementary Information for An Active Learning Workflow for Predicting Misfit Volume in Body-Centered Cubic Refractory High-Entropy Alloys

Shunshun Liu[1] **and Prasanna V. Balachandran**[1,*]

[1]University of Virginia, Department of Materials Science and Engineering, Charlottesville, 22903, USA
[*]pvb5e@virginia.edu

S1 Misfit Volume Calculation

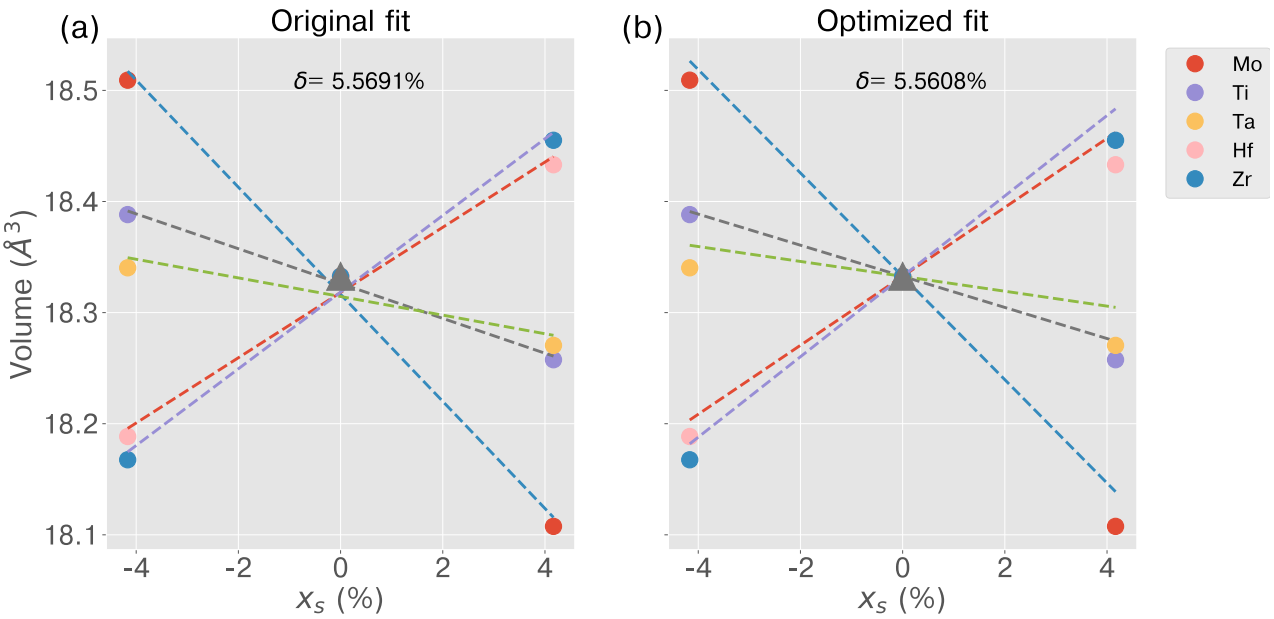

Figure S1. Elemental misfit volume (ΔV_n) fitting for the BCC HfMoTaTiZr RHEA. Each line is fit using three compositions, with ΔV_n extracted from the slope. (a) Unconstrained fit (original), in which each element's slope is determined independently. (b) Constrained fit (optimized), in which the slopes are determined subject to $\sum_n \Delta V_n = 0$.

S2 Active Learning and Machine Learning Performance

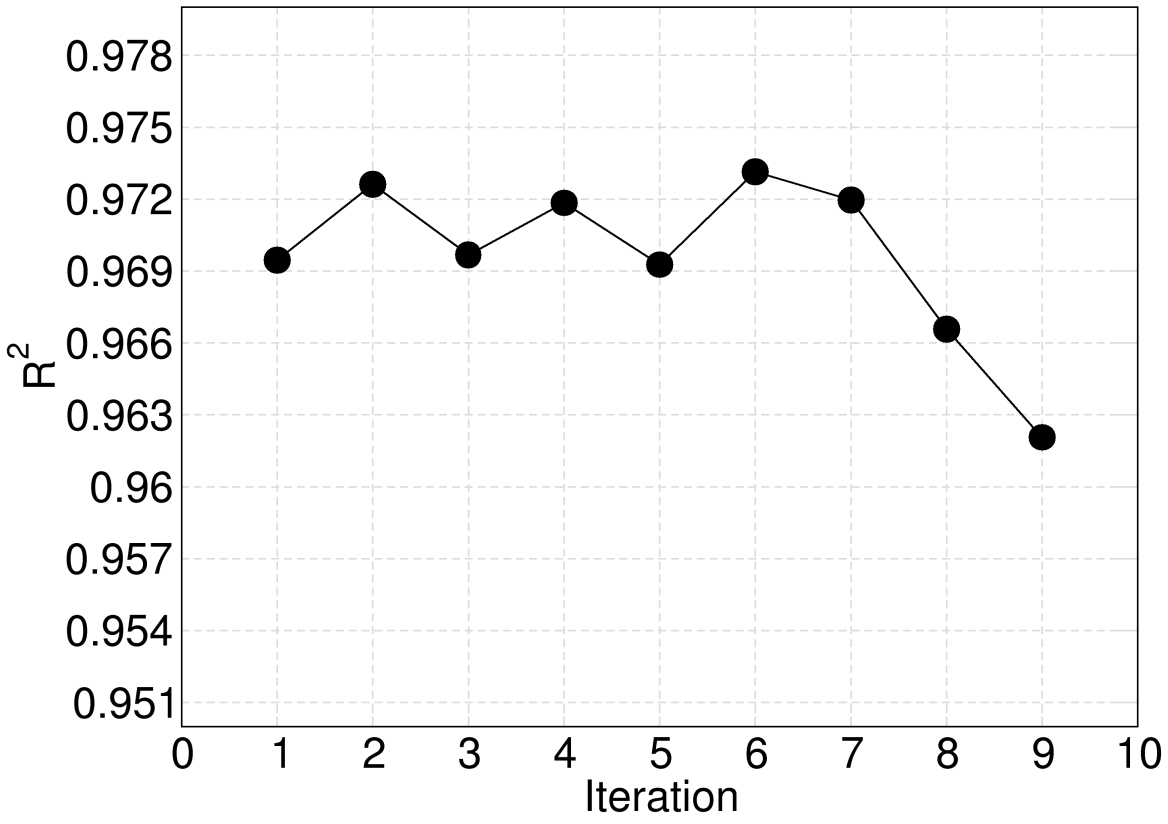

Figure S2. The training set R^2 score of the ensemble support vector regression (eSVR) model after each active learning iteration.

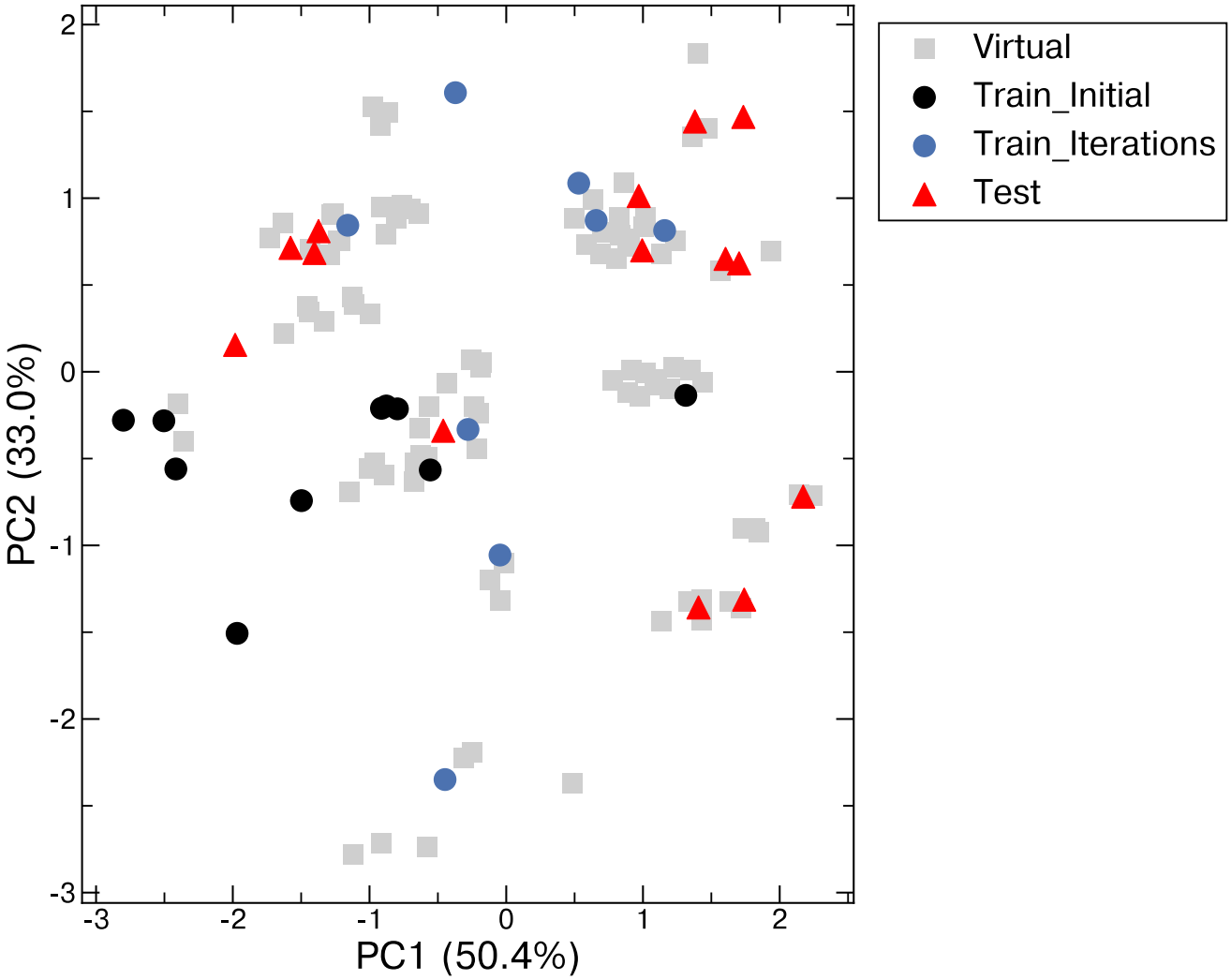

Figure S3. PCA projection of the dataset containing 126 compositions after the 9th active learning (AL) iteration. PC1 and PC2 account for 50.4% and 33.0% of the total variance, respectively. Gray squares denote unsampled candidates in the virtual library; black circles indicate the initial training set; blue circles mark new points recommended by the information-condensing active learning (ICAL) acquisition function over all AL iterations; and red triangles represent the independent test set drawn randomly from the design space.

S3 Global feature importance

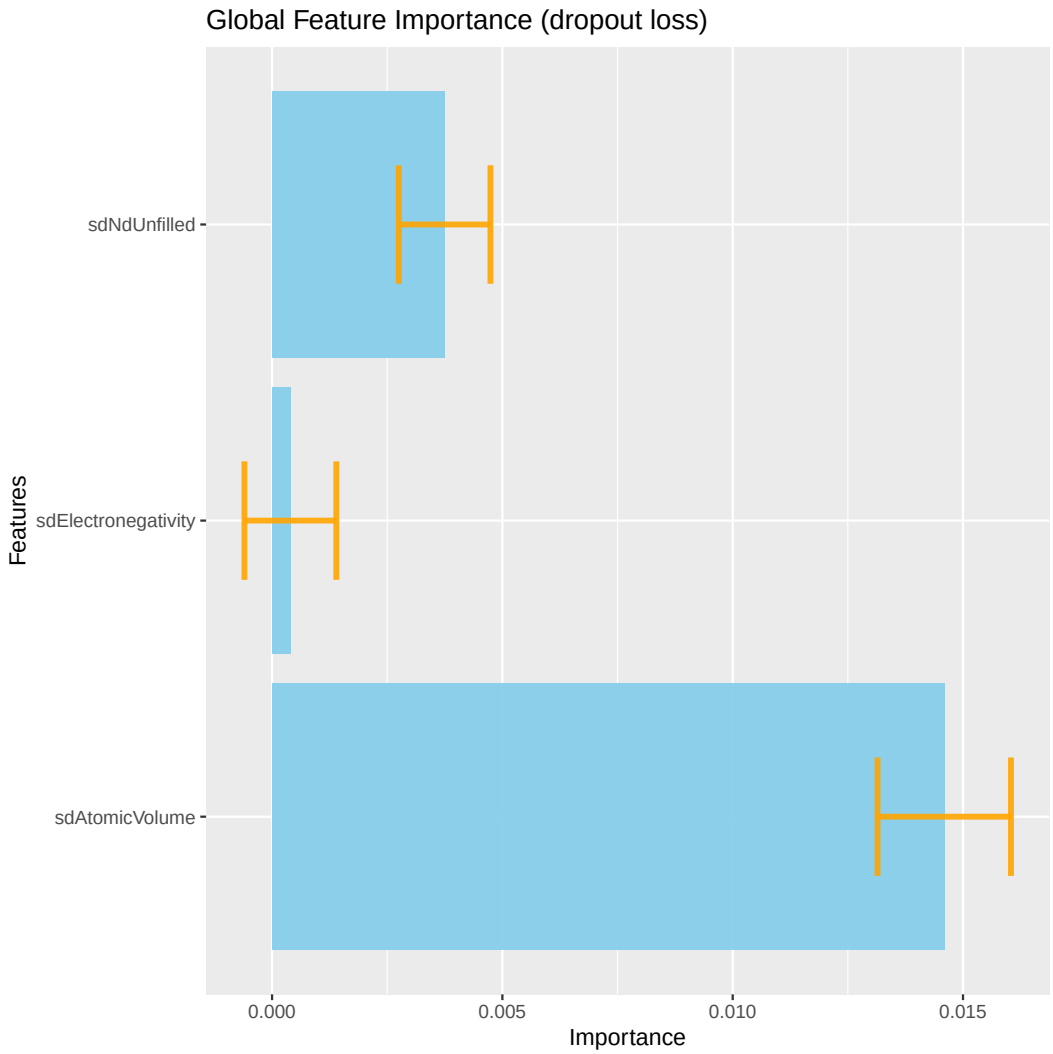

Figure S4. Permutation-based global feature importance scores after the 9th active learning iteration. Importance (x-axis) quantifies the relative contribution of each input feature to model performance, estimated by the decrease in predictive accuracy upon random permutation of that feature.

S4 Correlation with Other Descriptors of Atomic Mismatch

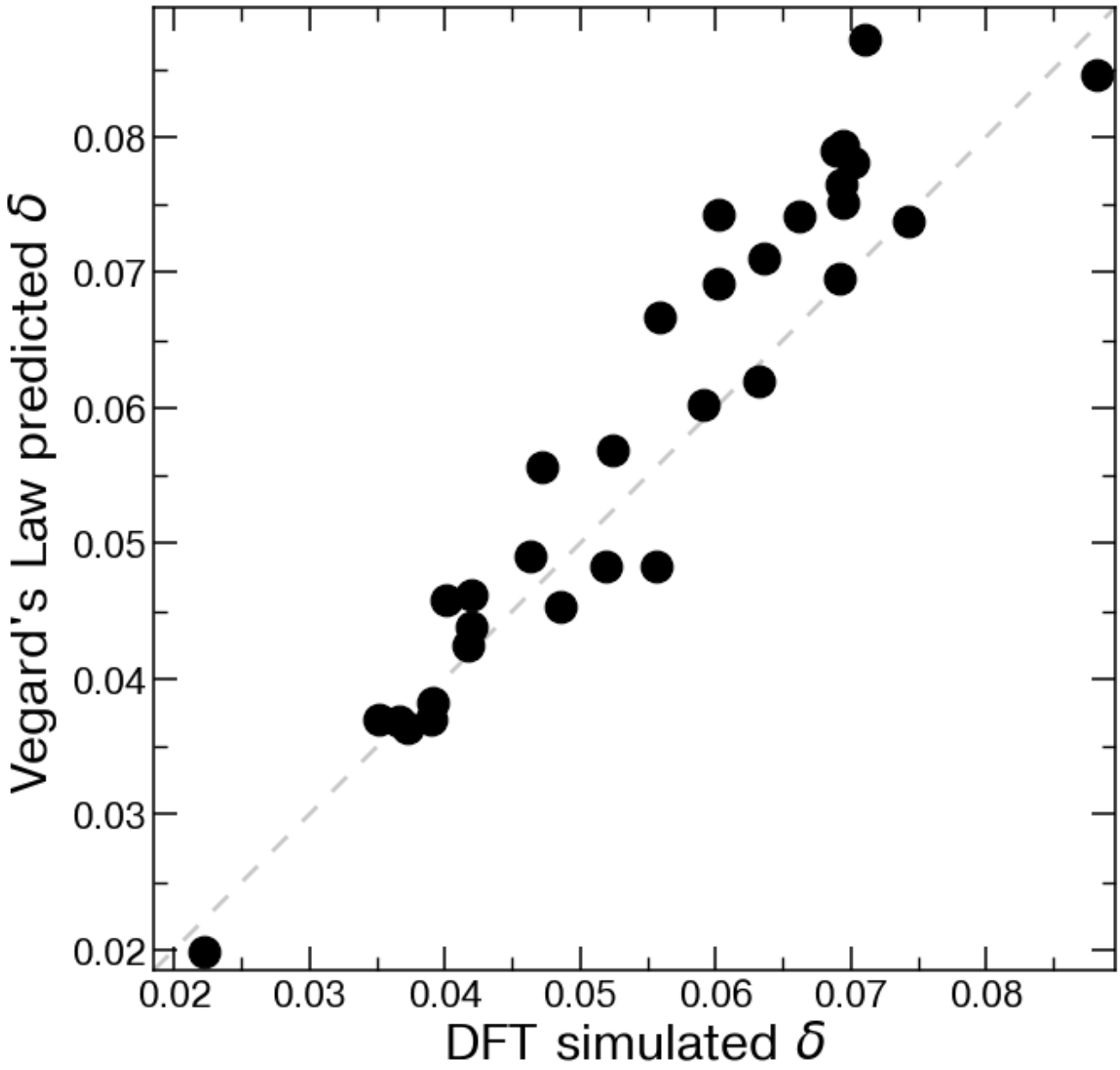

Figure S5. Parity plot comparing the Vegard's law approximated δ-descriptor (y-axis) against the DFT-simulated δ-descriptor (x-axis), with a coefficient of determination $R^2 = 0.81$.

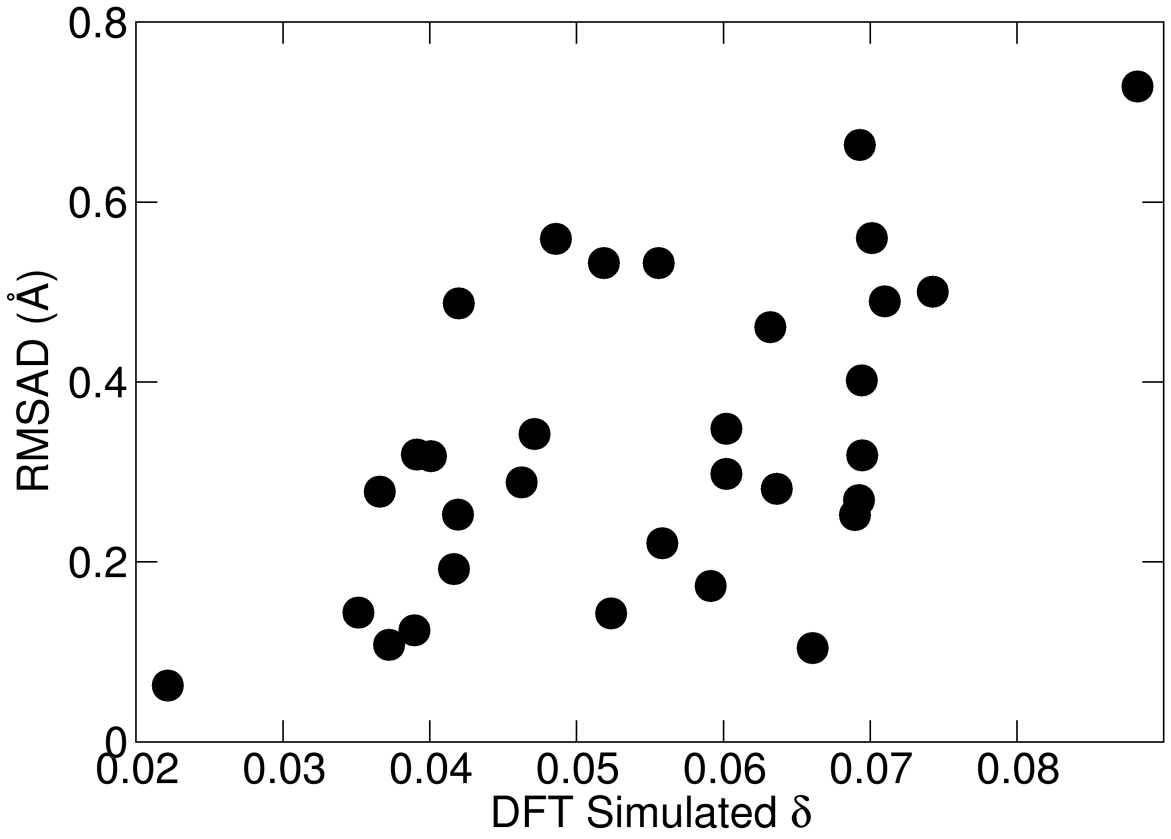

Figure S6. Correlation between the root mean square atomic displacement (RMSAD, *y*-axis) and the DFT-simulated δ-descriptor (*x*-axis), with a Pearson correlation coefficient (PCC) of 0.55.

S5 Room-Temperature Yield Strength Data

Table S1. Comparison of room-temperature yield strength (σ_y) between Maresa-Curtin mechanistic model predictions ($\sigma_y^{Mechanistic}$) and experiments ($\sigma_y^{Expt.}$) for equiatomic BCC RHEAs. (a) Zr- and Hf-free alloys; (b) Zr- and Hf-containing alloys. Mean $\sigma_y^{Mechanistic}$ and StdDev $\sigma_y^{Mechanistic}$ denote the predicted mean and standard deviation of the σ_y from the mechanistic model, respectively.

(a) Zr, Hf-free alloys

Alloy	Mean $\sigma_y^{Mechanistic}$ (MPa)	StdDev $\sigma_y^{Mechanistic}$ (MPa)	$\sigma_y^{Expt.}$ (MPa)	**Ref.**
MoNbTiV	1347	523	1200	Chen *et al.*[1]
MoNbTaVW	1478	402	1246	Senkov *et al.*[2]
MoNbTaW	1155	391	1058	Couzinié *et al.*[3]
MoTaTiV	1468	454	1221	Qiao *et al.*[4]
MoNbTaTiV	1445	483	1400	Yao *et al.*[5]
MoNbTaTiVW	1310	401	1515	Han *et al.*[6]
MoNbTaTiW	970	363	1343	Senkov *et al.*[7]
NbTaTiVW	1419	418	1420	Yao *et al.*[8]
NbTaVW	1671	462	1530	Yao *et al.*[8]
NbTaTi	1203	916	620	Zỳka *et al.*[9]

(b) Zr, Hf-containing alloys

Alloy	Mean $\sigma_y^{Mechanistic}$ (MPa)	StdDev $\sigma_y^{Mechanistic}$ (MPa)	$\sigma_y^{Expt.}$ (MPa)	**Ref.**
HfMoNbTaTiZr	2179	729	1512	Juan *et al.*[10]
HfMoTaTiZr	2395	773	1600	Juan *et al.*[11]
MoNbTiVZr	2549	986	1786	Zhang *et al.*[12]
MoNbTiZr	2228	835	1592	Zhang *et al.*[12]
HfNbTaZr	2133	796	1315	Maiti *et al.*[13]
HfTaTiZr	2225	811	1500	Huang *et al.*[14]
HfMoNbTiZr	2306	824	1575	Senkov *et al.*[7]
NbTiZr	2102	837	975	Couzinié *et al.*[3]
HfNbTiZr	2031	765	879	Couzinié *et al.*[3]
NbTaTiZr	2173	784	1144	Zỳka *et al.*[9]
HfMoNbTaZr	2488	795	1524	Tseng *et al.*[15]
HfMoNbTaTi	1877	589	1369	Tseng *et al.*[15]

References

1. Chen, S. Y., Yang, X., Dahmen, K. A., Liaw, P. K. & Zhang, Y. Microstructures and crackling noise of $Al_xNbTiMoV$ high entropy alloys. *Entropy* **16**, 870–884 (2014).
2. Senkov, O. N., Wilks, G. B., Scott, J. M. & Miracle, D. B. Mechanical properties of Nb25Mo25Ta25W25 and V20Nb20Mo20Ta20W20 refractory high entropy alloys. *Intermetallics* **19**, 698–706 (2011).
3. Couzinié, J.-P. *et al.* On the room temperature deformation mechanisms of a TiZrHfNbTa refractory high-entropy alloy. *Mater. Sci. Eng. A* **645**, 255–263 (2015).
4. Qiao, D. X., Jiang, H., Chang, X. X., Lu, Y. P. & Li, T. J. Microstructure and mechanical properties of $VTaTiMoAl_x$ refractory high entropy alloys. In *Materials science forum*, vol. 898, 638–642 (Trans Tech Publ, 2017).
5. Yao, H. *et al.* Mechanical properties of refractory high-entropy alloys: Experiments and modeling. *J. Alloy. Compd.* **696**, 1139–1150 (2017).
6. Han, Z. *et al.* Effect of Ti additions on mechanical properties of NbMoTaW and VNbMoTaW refractory high entropy alloys. *Intermetallics* **84**, 153–157 (2017).
7. Senkov, O. N., Gorsse, S. & Miracle, D. B. High temperature strength of refractory complex concentrated alloys. *Acta Materialia* **175**, 394–405 (2019).
8. Yao, H. *et al.* NbTaV-(Ti, W) refractory high-entropy alloys: Experiments and modeling. *Mater. Sci. Eng. A* **674**, 203–211 (2016).
9. Zỳka, J. *et al.* Microstructure and room temperature mechanical properties of different 3 and 4 element medium entropy alloys from HfNbTaTiZr system. *Entropy* **21**, 114 (2019).
10. Juan, C.-C. *et al.* Solution strengthening of ductile refractory $HfMo_xNbTaTiZr$ high-entropy alloys. *Mater. Lett.* **175**, 284–287 (2016).
11. Juan, C.-C. *et al.* Enhanced mechanical properties of HfMoTaTiZr and HfMoNbTaTiZr refractory high-entropy alloys. *Intermetallics* **62**, e83 (2015).
12. Zhang, Y., Yang, X. & Liaw, P. Alloy design and properties optimization of high-entropy alloys. *JOM* **64**, 830–838 (2012).
13. Maiti, S. & Steurer, W. Structural-disorder and its effect on mechanical properties in single-phase TaNbHfZr high-entropy alloy. *Acta Materialia* **106**, 87–97 (2016).
14. Huang, H. *et al.* Phase-transformation ductilization of brittle high-entropy alloys via metastability engineering. *Adv. Mater.* **29**, 1701678 (2017).
15. Tseng, K.-K. *et al.* Effects of Mo, Nb, Ta, Ti, and Zr on mechanical properties of equiatomic Hf-Mo-Nb-Ta-Ti-Zr alloys. *Entropy* **21**, 15 (2018).